Time-frequency analysis of seismic data using local attributes[a]

[a]Published in Geophysics, 76, no. 6, P23-P34, (2011)

Guochang Liu[*], *Sergey Fomel*[†], *Xiaohong Chen*[*]

ABSTRACT

Time-frequency analysis is an important technology in seismic data processing and interpretation. To localize frequency content in time, we have developed a novel method for computing a time-frequency map for nonstationary signals using an iterative inversion framework. We calculated time-varying Fourier coefficients by solving a least-squares problem that uses regularized nonstationary regression. We defined the time-frequency map as the norm of time-varying coefficients. Time-varying average frequency of the seismic data can also be estimated from the time-frequency map calculated by our method. We tested the method on benchmark synthetic signals and compared it with the well-known Stransform. Two field data examples showed applications of the proposed method for delineation of sand channels and for detection of low-frequency anomalies.

INTRODUCTION

Time-frequency decomposition maps a 1D signal into a 2D signal of time and frequency, and describes how the spectral content of the signal changes with time. Time-frequency analysis has been used extensively in seismic data processing and interpretation, including attenuation measurement (Reine et al., 2009), direct hydrocarbon detection (Castagna et al., 2003), and stratigraphic mapping (Partyka et al., 1998). The widely used short-time Fourier transform (STFT) method produces a time-frequency spectrum by taking the Fourier transform of data windows (Cohen, 1995), which leads to a tradeoff between temporal and spectral resolution.

Over the past two decades, wavelet-based methods have been applied to time-frequency analysis of seismic data. Chakraborty and Okaya (1995) compare wavelet-based with Fourier-based methods for performing time-frequency analysis on seismic data and showed that the wavelet-based method improves spectral resolution. The continuous-wavelet transform (CWT) provides a time-scale map, known as a scalogram (Rioul and Vetterli, 1991), rather than a time-frequency spectrum. Because a scale represents a frequency band, Hlawatsch and Boudreaux-Bartels (1992) choose their scale to be inversely proportional to the center frequency of the wavelet, which allowed them to transform their scalogram into a time-frequency map. Sinha et al.

(2005) provide a novel method of obtaining such a time-frequency map by taking a Fourier transform of the inverse CWT.

Wigner-Ville distribution (WVD) (Wigner, 1932) represents time-frequency components by using the reverse of the signal as an analysis window function. WVD varies resolution in the time-frequency plane by providing good temporal resolution at high frequencies and good frequency resolution at a low-frequency (Cohen, 1989). Applications of WVD are hindered by cross-term interference, which can be suppressed by using appropriate kernel functions. A smoothed pseudo-WVD with independent time and frequency functions as kernels achieves a relatively good resolution in both time and frequency (Li and Zheng, 2008). Wu and Liu (2009) employed smoothed pseudo-WVD with a Gaussian kernel function to reduce cross-term interference.

The S-transform is an invertible time-frequency analysis technique that combines elements of wavelet transforms and short-time Fourier transforms. The S-transform with an arbitrary and varying shape was applied to seismic data analysis by Pinnegar and Mansinha (2003). Matching pursuit (Mallat and Zhang, 1993), which was also applied in seismic signal analysis (Chakraborty and Okaya, 1995; Castagna et al., 2003; Liu et al., 2004; Liu and Marfurt, 2005; Wang, 2007), decomposes a seismic trace into a series of wavelets that belong to a comprehensive dictionary of functions. These wavelets are selected so as to best match signal structures. The spectrum of the signal is then the time-shifted sum of each of the wavelets.

Local attributes (Fomel, 2007a) can adaptively measure timevarying seismic signal characteristics in the neighborhood of each data point. Local attributes have been successfully applied to seismic image registration (Fomel and Jin, 2009), phase detection (van der Baan and Fomel, 2009; Fomel and van der Baan, 2009), and stacking (Liu et al., 2009, 2011b). A natural extension of local attributes, regularized nonstationary regression, decomposes input data into a number of nonstationary components (Fomel, 2009; Liu and Fomel, 2010; Liu et al., 2011a).

In this paper, we propose a new method of time-frequency analysis in which we use time-varying Fourier coefficients to define a time-frequency map. As in regularized nonstationary regression, shaping regularization (Fomel, 2007b) constrains continuity and smoothness of the coefficients. Given the close connection between Fourier transforms and the least-squares norm, the least-squares approach to time-frequency analysis is not new, having been used previously, for example, by Youn and Kim (1985). What is novel about our approach is the use of regularization for explicitly controlling the time resolution of time-frequency representations.

The paper is organized as follows.We first describe the proposed method for time-frequency analysis. Then we show how to compute the time-varying average frequency from the time-frequency map. We use benchmark synthetic examples to test the performance of the proposed method. Finally, we apply the proposed method to channel detection and low-frequency anomaly detection in field seismic data.

TIME-FREQUENCY ANALYSIS USING LOCAL ATTRIBUTES

The Fourier transform has found various applications in signal analysis. The classic Fourier transform indicates the presence of different frequencies within the analysis window, but does not show where in that window the particular frequency components reside. Localized frequency information can be obtained by computing the Fourier transform with a temporally shifted window. Such an approach to time-frequency analysis is known as the STFT (Allen, 1977). The window function is commonly parameterized by window size, overlap, and taper. Once the window function has been chosen for the STFT, temporal and spectral resolutions are fixed for the entire time-frequency map.

The S-transform (Stockwell et al., 1996) is similar to the STFT, but with a Gaussian-shaped window whose width scales inversely with frequency. The expression of the S-transform is

$$S(\tau, f) = \int_{-\infty}^{\infty} S(t) \left\{ \frac{|f|}{\sqrt{2\pi}} \exp\left[\frac{-f^2(\tau - t)^2}{2} \right] \exp(-2\pi i f t) \right\} dt, \tag{1}$$

where $s(t)$ is a signal and τ is a parameter which controls the position of the Gaussian window. The S-transform is conceptually a hybrid of the STFT and wavelet analysis, containing elements of both but having its own properties. Like STFT, the S-transform uses a window to localize the complex Fourier sinusoid, but, unlike the STFT and analogously to the wavelet transform, the width of the window scales with frequency.

Consider a signal $f(x)$ on $[0, L]$. The Fourier series, assuming a periodic extension of the boundary conditions, can be expressed as

$$f(t) \approx a_0 + \sum_{k=1}^{\infty} \left[a_k \cos\left(\frac{2k\pi t}{L} \right) + b_k \sin\left(\frac{2k\pi t}{L} \right) \right], \tag{2}$$

where a_k and b_K are the series coefficients. The relationship between k and frequency f is $k = Lf$. In the case of the discrete Fourier transform, frequency is finite. Letting $\mathbf{\Psi}_k(t)$ represent the Fourier basis

$$\mathbf{\Psi}_k(t) = \begin{bmatrix} \mathbf{\Psi}_{1k}(t) \\ \mathbf{\Psi}_{2k}(t) \end{bmatrix} = \begin{bmatrix} \cos\left(\frac{2k\pi t}{L}\right) \\ \sin\left(\frac{2k\pi t}{L}\right) \end{bmatrix}, \tag{3}$$

and $\mathbf{C}_k$ represent the series coefficients

$$\mathbf{C}_k = \begin{bmatrix} a_k & b_k \end{bmatrix}, \tag{4}$$

where $b_0 = 0$, equation 1 can be written as

$$f(t) = \sum_{k=0}^{\infty} \mathbf{C}_k \mathbf{\Psi}_k(t). \tag{5}$$

If frequency is finite, the range of k becomes $[0, N]$, $N = k_{max} = Lf_{max}$. In linear notation, $\mathbf{C}_k$ can be obtained by solving the least-squares problem

$$\min_{\mathbf{C}_k} \left\| f(t) - \sum_{k=0}^{N} \mathbf{C}_k \mathbf{\Psi}_k(t) \right\|_2^2, \tag{6}$$

where ||||denotes the squared $L-2$ norm of a function. By allowing coefficients $\mathbf{C}_k$ to change with time t, we can define the timevarying coefficients $\mathbf{C}_k(t)$ via the following least-squares problem

$$\min_{\mathbf{C}_k} \sum_{k=0}^{N} ||f(t) - \mathbf{C}_k \mathbf{\Psi}_k(t)||_2^2 . \tag{7}$$

The Fourier coefficient $\mathbf{C}_k(t)$ in equation 7 is a function of time t and frequency $f = kL$ and $\mathbf{C}_k(t) = [a_k \quad b_k]$. The numerical support of frequency f can be between zero and the Nyquist frequency (Cohen, 1995), and the interval of frequency can be $\Delta f = 1L$. In practical applications, the range of frequencies can also be assigned by the user. In matrix notation, equation 7 can be written as

$$[f(t) \quad f(t)... \quad f(t)]^T \approx [D\{\mathbf{\Psi}_1(t) \quad ... \quad \mathbf{\Psi}_N(t)\}] [\mathbf{C}_1(t) \quad ... \quad \mathbf{C}_N(t)]^T , \tag{8}$$

where $D\{...\}$ denotes a diagonal matrix which is composed from the elements of $\mathbf{Psi}_k(t)$.

The problem of minimization in equation 7 is mathematically ill-posed because it is severely underconstrained: There are more unknown variables than constraints. To solve this ill-posed problem, we force the coefficients $\mathbf{C}_k(t)$ to have a desired behavior, such as smoothness. With the addition of a regularization term, equation 7 becomes

$$\min_{\mathbf{C}_k(t)} \sum_{k=0}^{N} ||f(t) - \mathbf{C}_k(t) \mathbf{\Psi}_k(t)||_2^2 + R[\mathbf{C}_k(t)] , \tag{9}$$

where R denotes the regularization operator. If we use classic Tikhonov regularization (Tikhonov, 1963), equation 9 can be written as

$$\min_{\mathbf{C}_k(t)} \sum_{k=0}^{N} ||f(t) - \mathbf{C}_k(t) \mathbf{\Psi}_k(t)||_2^2 + \varepsilon^2 \sum_{k=0}^{N} ||\mathbf{D}[\mathbf{C}_k(t)]||_2^2 , \tag{10}$$

where $\mathbf{D}$ is the Tikhonov regularization operator (roughening operator) and ε is a scalar regularization parameter.

Shaping regularization (Fomel, 2007b) provides a particularly convenient method of enforcing smoothness in iterative optimization schemes. In the appendix, we review the method of shaping regularization in detail. Fomel (2009) used shaping regularization to constrain the problem of nonstationary regression. In this paper, we use shaping regularization, analogous to the problem of nonstationary regression, to constrain estimated coefficients. We choose our shaping operator to be Gaussian smoothing with an adjustable radius. In shaping regularization, the radius of the Gaussian smoothing operator controls the smoothness of coefficients $\mathbf{C}_k(t)$.

Once we obtain time-varying Fourier coefficients $\mathbf{C}_k(t) = [a_k(t) \quad b_k(t)]$, the time-frequency map is defined as

$$F(t, f = k/L) = \sqrt{a_k^2(t) + b_k^2(t)}. \tag{11}$$

It is also possible to do an invertible time-frequency transform, as shown by Liu and Liu and Fomel (2010).

Consider a simple signal (Figure 1(a)), which includes three monophonic components at 10, 20, and 30 Hz and two broad-band spikes at 2 and 2.3 s. Time-frequency maps generated by the S-transform and our method are shown, respectively, in Figure 1(b) and 1(c). Frequency components appear to be represented well from low to high frequencies in the proposed method. In comparison with the S-transform, the proposed method provides superior resolution for monophonic waves. At the lower frequencies, the S-transform is as good as the proposed method on the spectral resolution for monophonic waves. Note that the S-transform represents spikes better at high frequencies. However, because the width of analysis window is large at low frequencies, the S-transform provides poor time resolution at low frequencies for spikes. When we use the shaping operator as a regularization term, there is an edge effect from smoothing, which appears near 0 s and 4 s (Figure 1(c)). Figure 1(d) displays the time-frequency map using a different parameter (30-point smoothing radius) to demonstrate adjustable time-frequency representation of the proposed method.

To show the effect of varying frequencies, we provide a composite chirp signal (Figure 2(a)), which includes two parabolic frequencies, each having a constant amplitude. Figure 2(b) and 2(c) shows the results of the S-transform and the proposed method with 10-point smoothing radius, respectively. The two frequency components are detected with higher time and frequency resolution by our method. The S-transform has high spectral resolution near low frequencies, but loses resolution at high frequencies. Resolution of the time-frequency map deteriorates in both methods when the curvature of the time-frequency curve becomes large (as indicated by the arrow).

In the proposed method, the smoothing radius used in shaping regularization is a parameter which controls the smoothness of the model. It is different from the method of the STFT and the S-transform, in which division into local windows is applied to the data to localize frequency content in time. In contrast to the wavelet-based methods (Chakraborty and Okaya, 1995; Sinha et al., 2005; Wang, 2007), our method, as a straightforward extension of the classic Fourier analysis, is different because of the choice of basis functions. The wavelet-based methods need to decide the wavelets, which can be regarded as patterns of seismic data. The closer the selected wavelets are to the true pattern of the input data, the better the result of the time-frequency analysis. In this paper, we use more general Fourier basis functions to compute the time-frequency map.

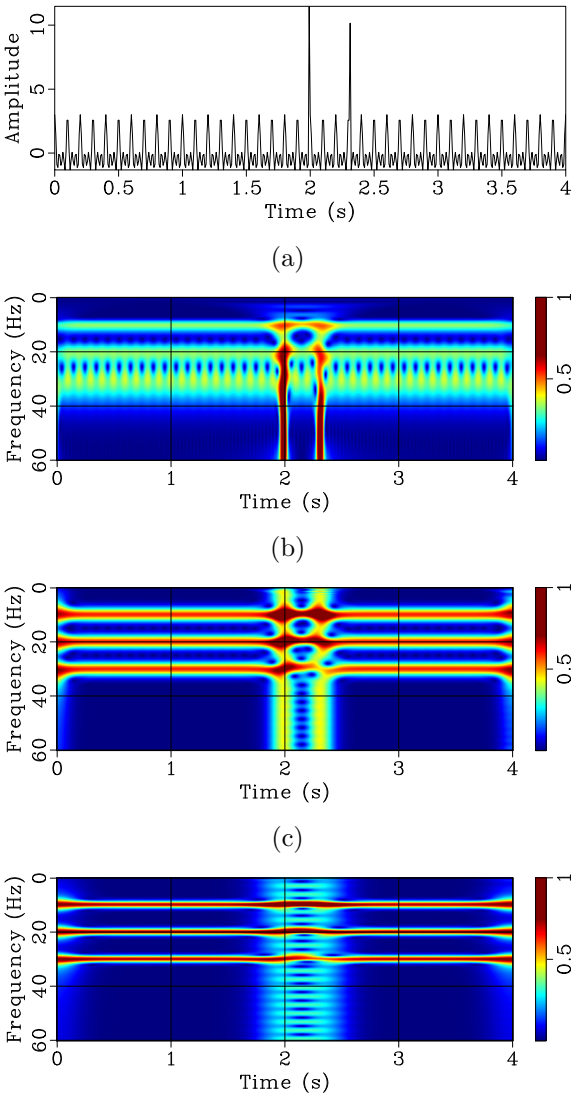

Figure 1: (a) Synthetic signal with three constant frequency components and two spikes. (b) Time-frequency map of the S-transform. (c) Time-frequency map of the proposed method with smoothing radius of 15 points. (d) Time-frequency map of the proposed method with smoothing radius of 30 points.

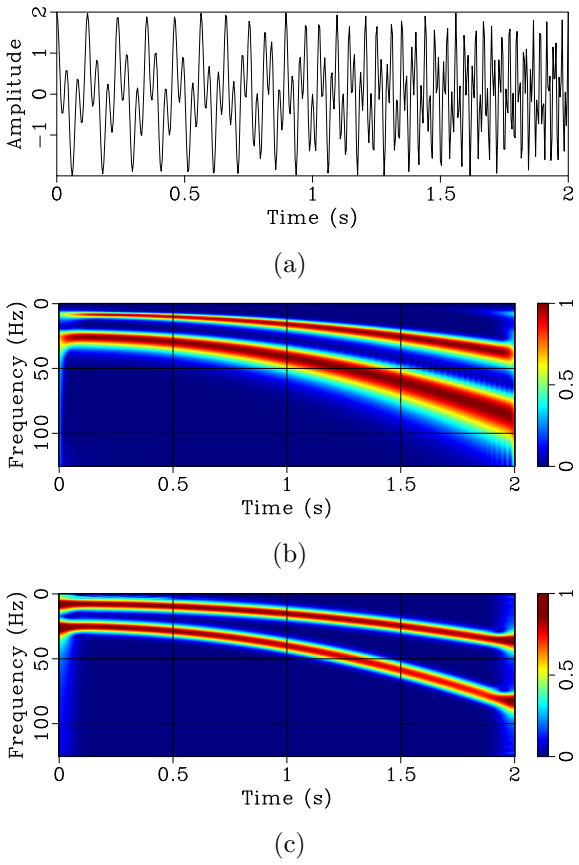

Figure 2: (a) Synthetic chirp signal with two parabolic frequency changes. (b) Time-frequency map of the S-transform. (c) Time-frequency map of the proposed method.

ESTIMATION OF TIME-VARYING AVERAGE FREQUENCY

Seismic instantaneous frequency is the derivative of the instantaneous phase

$$f_i(t) = \frac{1}{2\pi}\frac{d\phi(t)}{dt}, \tag{12}$$

where $\phi(t)$ is the instantaneous phase. Instantaneous frequency can be estimated directly using a discrete form of equation 12. This estimate is highly susceptible to noise. Fomel (2007a) modified the definition of instantaneous frequency to that of a local frequency by recognizing it as a form of regularized inversion, and by using regularization to constrain continuity and smoothness of the output.

Average frequency can be estimated from the time-frequency map (Claasen and Mecklenbruker, 1980; Cohen, 1989; Hlawatsch and Boudreaux-Bartels, 1992; Steeghs and Drijkoningen, 2001; Sinha et al., 2009). Average frequency at a given time is

$$f_a(t) = \frac{\int f F^2(f,t) df}{\int F^2(f,t) df}, \tag{13}$$

where $F(f,t)$ is the time-frequency map. Average frequency measured by equation 13 is the first moment along the frequency axis of a time-frequency power spectrum. Saha (1987) and Brian et al. (1993) analyzed the relationship between instantaneous frequency and the time-frequency map in detail. Extraction of the attributes from the time-frequency map of the seismic trace leads to considerable improvement of the signal-to-noise ratio of the attributes (Steeghs and Drijkoningen, 2001). We therefore propose applying equation 13 to our time-frequency map to compute the time-varying average frequency.

We used a synthetic nonstationary seismic trace to illustrate our approach to estimating time-varying average frequency. Figure 3(b) shows a synthetic seismic trace generated by nonstationary convolution (Margrave, 1998) of a random reflectivity series (Figure 3(a)) using a Ricker wavelet, the dominant frequency of which is a function of time, $f_d = 25t^2 + 15$. Figure 9 shows the scaled spectrum of the Ricker wavelet. Both the dominant frequency (white line in Figure 9 and the bandwidth increase with time. We computed the average frequency (black line in Figure 9 using equation 13 from the scaled spectrum of Ricker wavelets. We note that average frequency is larger than the dominant frequency at high frequencies for Ricker wavelets.

We generated the time-frequency map of the synthetic nonstationary seismic trace using the S-transform (Figure 4(b)) and the proposed method with a 10-point smoothing radius (Figure 4(c)). We observe that the time-frequency map by the proposed method has a bandwidth more similar to that of the time-frequency map of the Ricker wavelet (Figure 9), especially at the high frequencies. We estimated time-varying average frequency curves from the time-frequency map by the proposed

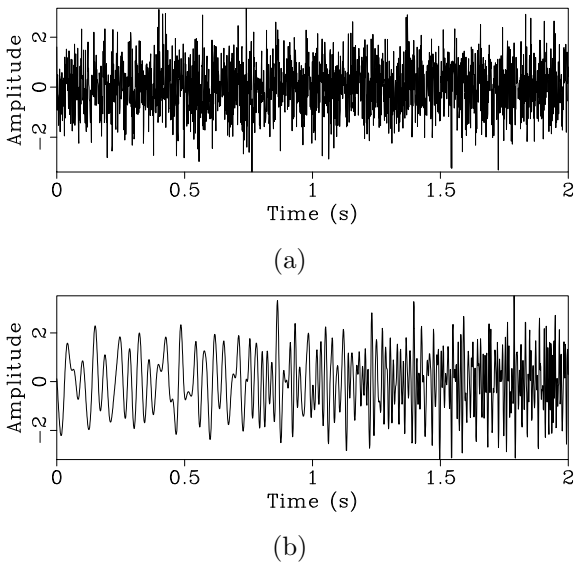

Figure 3: (a) Random reflectivity series. (b) Synthetic seismic trace.

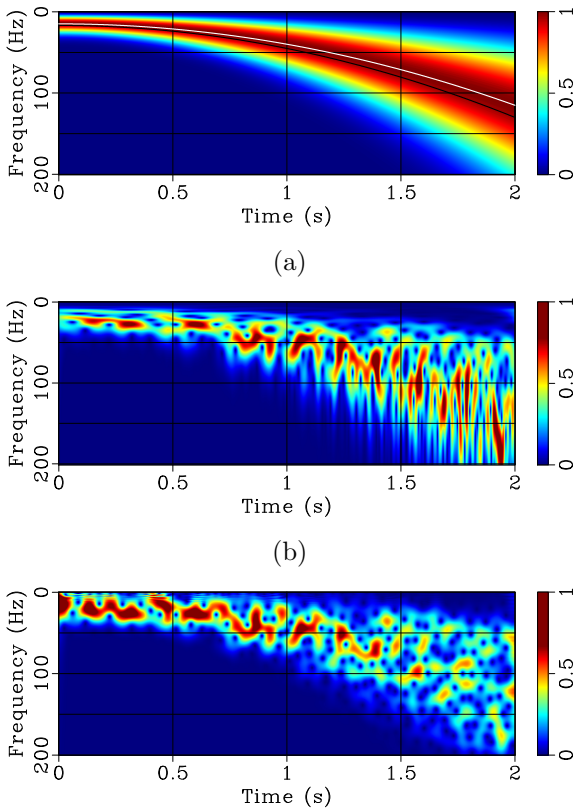

Figure 4: (a) Theoretical time-frequency map, which is scaled by a maximum in the frequency axis. White and black lines indicate dominant frequency and average frequency of Ricker wavelet, respectively. (b) Time-frequency map of the S-transform. (c) Time-frequency map of the proposed method.

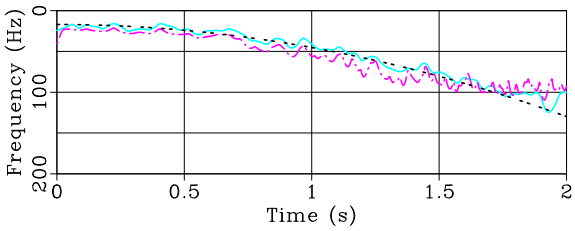

Figure 5: Time-varying average-frequency estimation (blue solid curve: estimated by our method; pink dashed curve: estimated by S-transform; black dot-dashed curve: theoretical curve, which is denoted by black line in Figure 9).

method (blue solid curve in Figure 5) and S-transform (pink dashed curve in Figure 5), respectively. Compared with the theoretical curve (black dashed curve in Figure 5), which was computed using equation 13 on the scaled spectrum of Ricker wavelets (Figure 9), the time-varying average frequency estimated by the proposed method is closer to the theoretical one.

EXAMPLES

We demonstrate the effectiveness of the proposed time-frequency analysis on a benchmark synthetic data set and two field data sets. We first use a synthetic seismic trace to illustrate how the proposed method obtains a time-frequency map, and then we test our method on two field data sets with applications to detecting channels and low-frequency anomalies.

Synthetic data

A synthetic seismic trace (Figure 6(a)) was obtained by adding Ricker wavelets with different frequencies and time shifts. The first event is an isolated wavelet with a frequency of 30 Hz, and the second event consists of a 15-Hz wavelet and a 60-Hz wavelet overlapping in time. The last event is a superposition of two 50-Hz wavelets with different arrival times. Figure 6(b) and 6(c) show the time-frequency maps by the S-transform and our method with 15-point smoothing radius, respectively. From the time-frequency map of the first event at 0.2 s, we found that time duration is long at low-frequency in the S-transform. The proposed method produces a more temporally limited ellipsoid spectrum for the first event. Note that the proposed method has higher spatial resolution at 0.6 s and temporal resolution at 1 s. This simple test shows that our method can be effective in representing

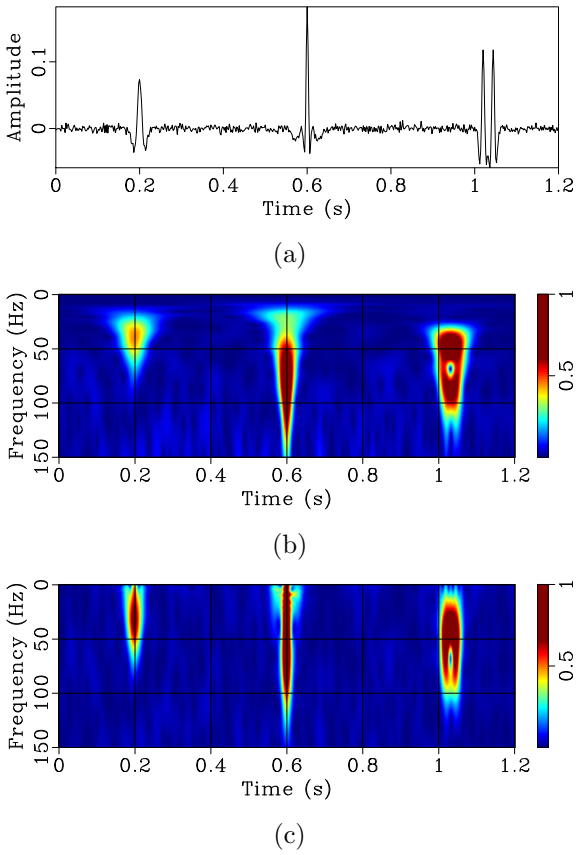

Figure 6: (a) Synthetic seismic trace. (b) Time-frequency map of the S-transform. (c) Time-frequency map of the proposed method.

3D Gulf of Mexico data for channel detection

Detecting channel structures is a common application of spectral decomposition (Partyka et al., 1998). Different frequency slices show different stratigraphic features. Figure 7 shows field data from the Gulf of Mexico (Lomask et al., 2006). To generate stratal slices (Zeng et al., 1998), we flattened this data set using predictive painting (Fomel, 2010). The flattened data set is shown in Figure 8. The flattening procedure can remove structural distortions and allows the interpreter to see geologic features as they were emplaced (Lomask et al., 2006). Predictive painting does a careful job of restoring true geological frequencies, as is evident from vertical sections. Figure 9 shows the average spectrum of the data set before flattening (dashed blue curve) and after flattening (solid red curve). We calculated the spectral decomposition of flattened data using the proposed method with a five-point smoothing radius. Figure 10 shows horizon slices from six different volumes at the same level in reference time. The horizontal blue lines on Figure 8b and 8c identify where the time slice is. Comparing seismic amplitudes (Figure 10a) with spectral decomposition at different frequencies (Figures 10b-f), several channels in 30 Hz slice are easily visible. The high-frequency spectral-decomposition maps, such as the 30-, 40-, and 50-Hz slices, can highlight detailed geologic features.

2D data example for low-frequency anomaly detection

Low-frequency anomalies are often attributed to abnormally high attenuation in gas-filled reservoirs and can be used as a hydrocarbon indicator (Castagna et al., 2003). A number of studies have investigated possible mechanisms of low-frequency anomalies associated with hydrocarbon reservoirs, but no adequate explanation is accepted absolutely (Ebrom, 2004; Kazemeini et al., 2009).

Figure 11 shows a poststack field data set with a bandwidth of about 10150 Hz (Figure 12).We used our proposed method with a ten-point smoothing radius to generate a time-frequency spectral map. Figure 13 shows the time-frequency map of one trace from the field data set. Note that our method has a higher temporal resolution than that of the S-transform, especially at 0.6-0.8 s.We can observe a general decay of frequency with time caused by seismic attenuation from the time-frequency map of one trace (Figure 13). The low-frequency anomaly is shown at 1.2-1.3 s (arrows). Figures 14 and 15 show single-frequency sections at 15, 31, and 70 Hz from two methods, the S-transform and the proposed method. We further found that the proposed method provides higher temporal and spatial resolution, especially in low-frequency sections. Figures 14(a) and 15(a) both show high-amplitude, low-frequency anomalies (ellipse). However, these anomalies gradually disappear in the high-frequency section (Figures 14(b) and 14(c) and 15(b) and 14(c)). Note that the spatial resolution of low-frequency anomalies in the proposed method (Figure 15(a)) is higher than that in the S-transform (Figure 14(a)). We also computed the time-varying average frequency section for this example using equation 13 (Figure

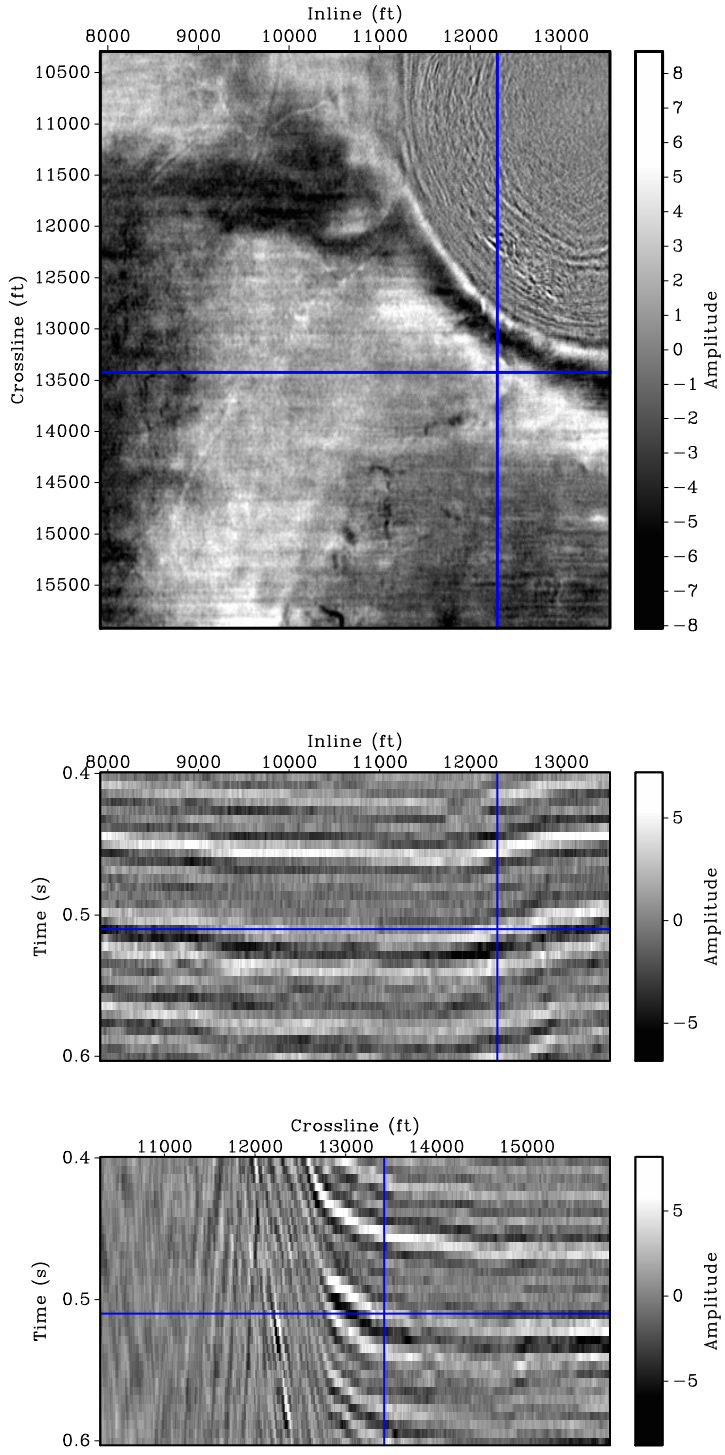

Figure 7: Seismic image from Gulf of Mexico. (a) Time slice. (b) Inline section. (c) Crossline section. Blue lines in (a) identify the location of inline and crossline sections. The horizontal blue lines in (b) and (c) identify where the time slice is.

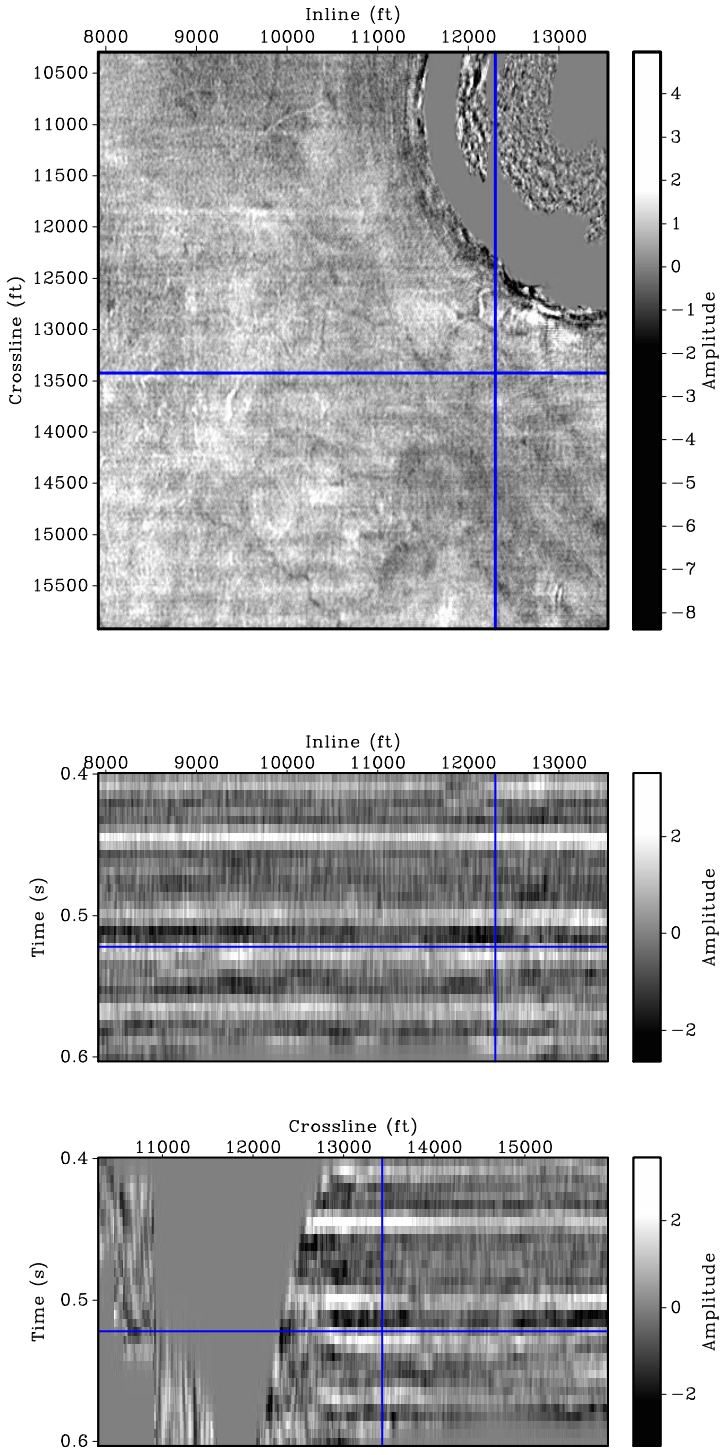

Figure 8: Seismic image from Figure 7 after flattening by predictive painting. (a) Time slice. (b) Inline section. (c) Crossline section. The blue lines on (a) identify the location of inline and crossline sections. The horizontal blue lines on (b) and (c) identify where the time slice is.

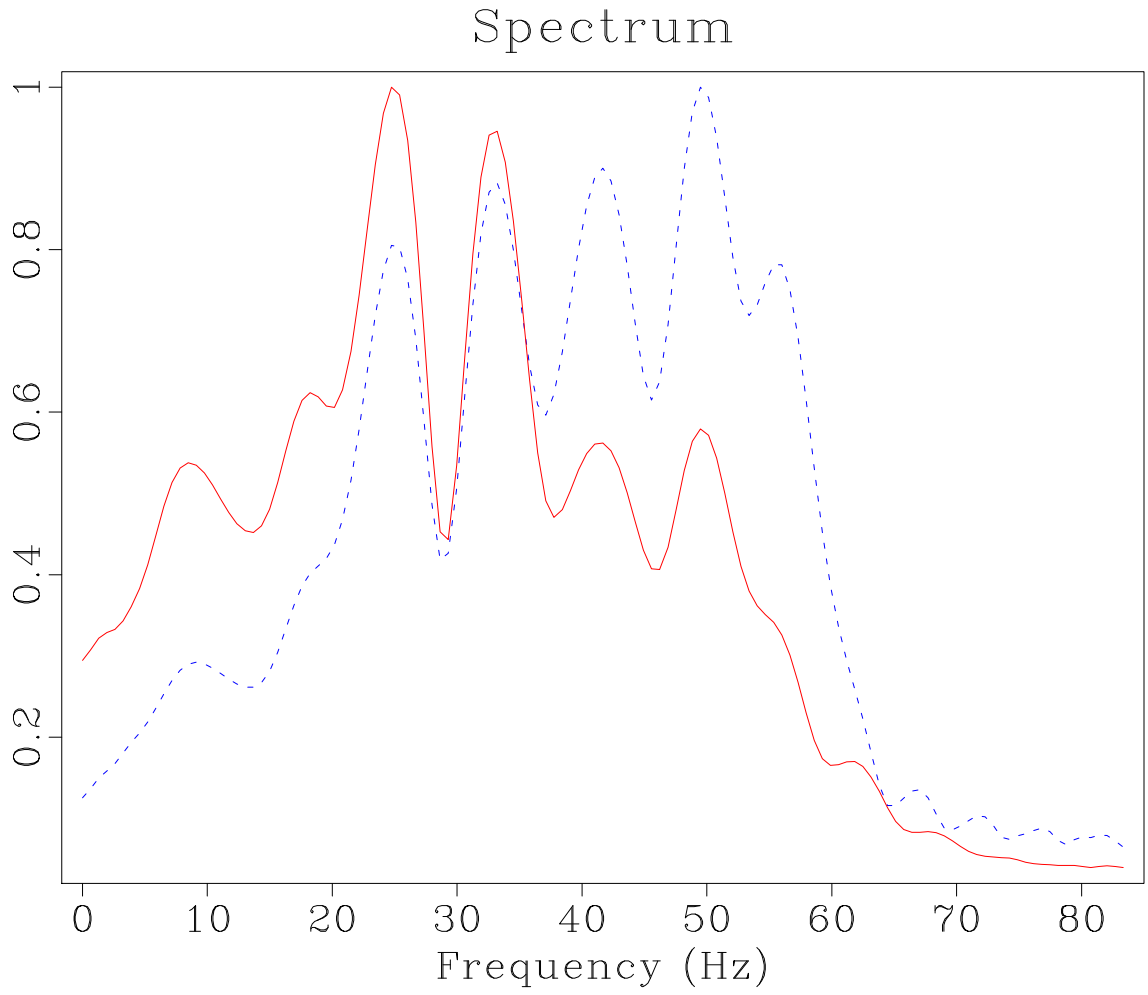

Figure 9: Average data spectrum before flattening (dashed blue curve) and after flattening (solid red curve).

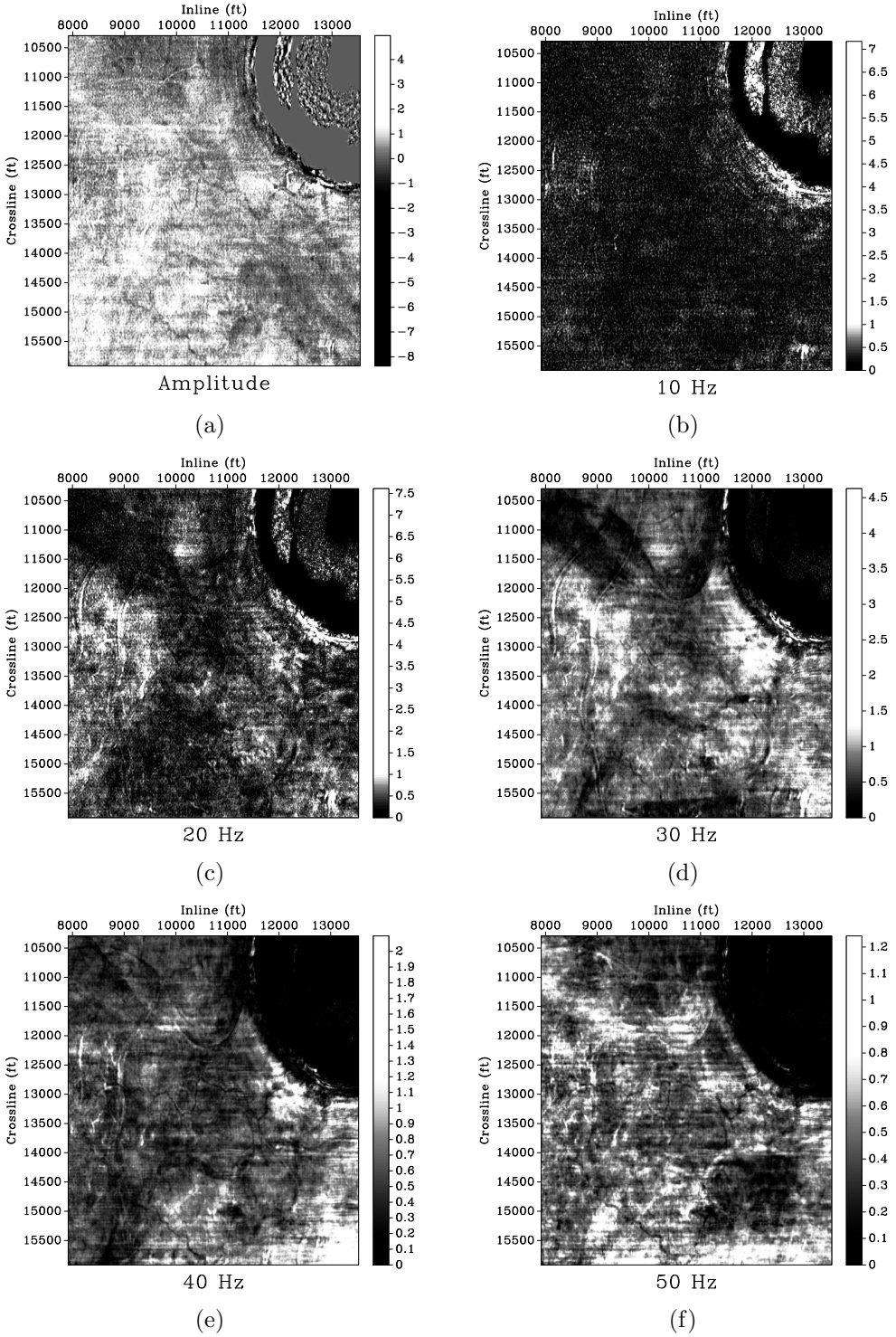

Figure 10: Comparison of horizon slices, from four different volumes at the same level: (a) conventional amplitude; and spectraldecomposition at (b) 10 Hz, (c) 20 Hz, (d) 30 Hz, (e) 40 Hz, and (f) 50 Hz. The slice of 30 Hz displays most clearly visible channel features.

16). We find that the average frequency is about 60 Hz in shallow layers, but 25 Hz in deep layers. The average frequency of low-frequency anomalies is very low, just about 15 Hz. This example shows that comparison of single low-frequency sections from the proposed method is able to detect low-frequency anomalies that might be caused by hydrocarbons, as demonstrated in other studies (Castagna et al., 2003; Korneev et al., 2004; Zhenhua et al., 2008). What we demonstrate by this example is that the proposed method can be used to detect low-frequency anomalies in seismic sections. Well control is generally needed to interpret this section more accurately.

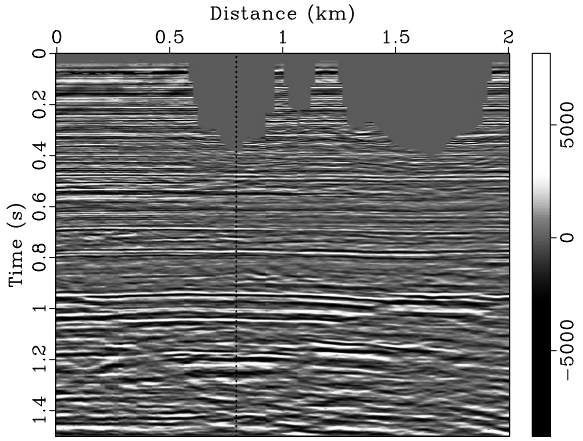

Figure 11: A field marine seismic data set.

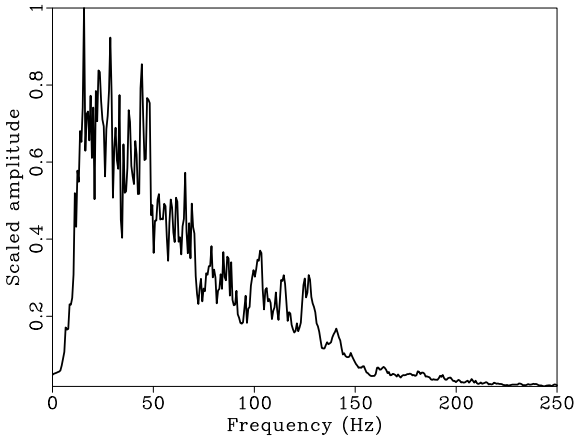

Figure 12: The averaged Fourier spectra of the field data.

CONCLUSION

We have presented a novel numerical method for computing time-frequency representation using least-squares inversion with shaping regularization. This time-frequency-analysis technology can be applied to nonstationary signal analysis. The method is a straightforward extension of the classic Fourier analysis. The parameter used in

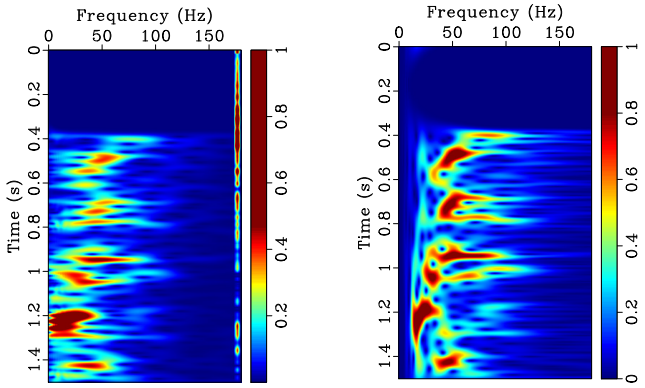

(a) (b)

Figure 13: Time-frequency map of one trace (denoted by black line in Figure 12). (a) S-transform; (b) the proposed method.

shaping regularization, the radius of the Gaussian smoothing operator, controls the smoothness of time-varying Fourier coefficients. The smooth time-varying average frequency attribute can also be estimated from the proposed time-frequency analysis technology. We have demonstrated applications of the proposed time-frequency analysis for detecting channels and lowfrequency anomalies in seismic images. Finally, we realize that many different algorithms are capable of computing time-frequency representations. We have provided some comparisons of our method with one of them (the S-transform) but cannot make the comparison exhaustive and do not claim that our method will necessarily perform better in all practical situations. Both approaches to time-frequency analysis have advantages and disadvantages. What we see as the main advantages of our method are its conceptual simplicity, computational efficiency, and explicit controls on time and frequency resolution.

ACKNOWLEDGMENTS

We would like to thank Thomas J. Browaeys, Yang Liu, and Mirko van der Baan for inspiring discussions, and the China Scholarship Council (grant 2007U44003) for partial support of the first authors research. This work is financially supported by the National Basic Research Program of China (973 program, grant 2007CB209606) and by the National High Technology Research and Development Program of China (863 program, grant 2006AA09A102-09).We also thank associate editor Kurt J. Marfurt and three anonymous reviewers for their constructive comments, which improved the quality of the paper.

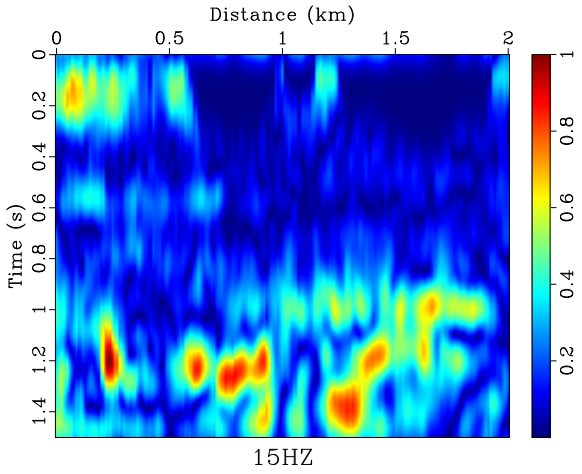

(a)

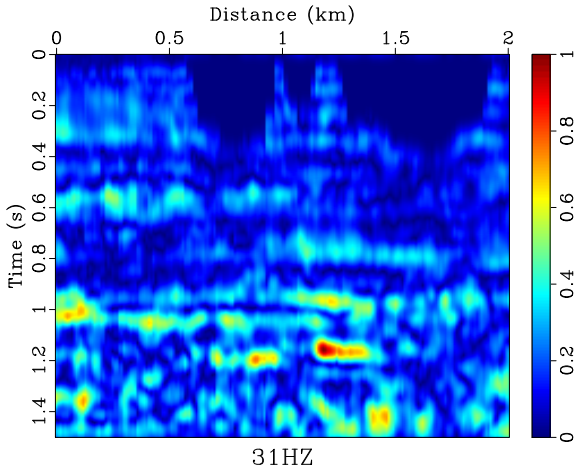

(b)

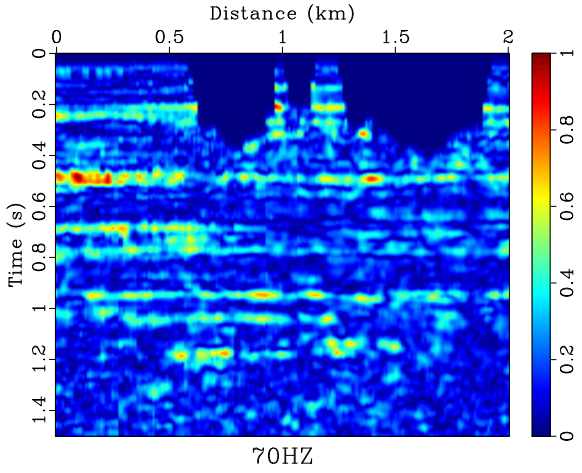

(c)

Figure 14: Comparison of common-frequency slices from S-transform; (a) 10 Hz, (b) 31 Hz, and (c) 70 Hz. The lowfrequency abnormality is indicated by an ellipse.

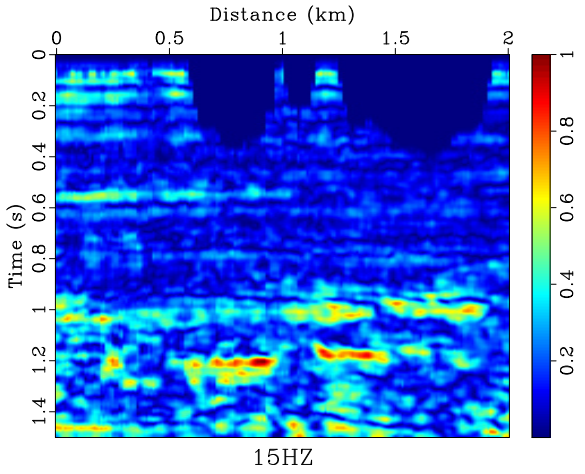

(a)

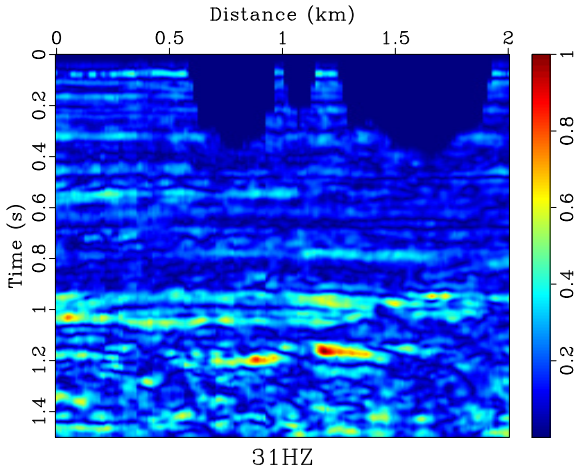

(b)

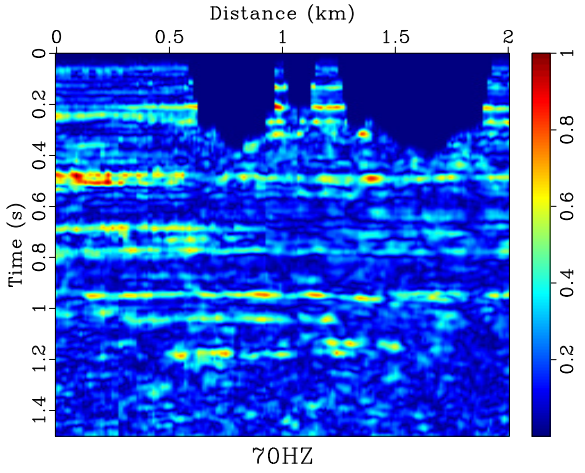

(c)

Figure 15: Comparison of common-frequency slices from the proposed method; (a) 10 Hz, (b) 31 Hz, and (c) 70 Hz. The lowfrequency abnormity is indicated by an ellipse.

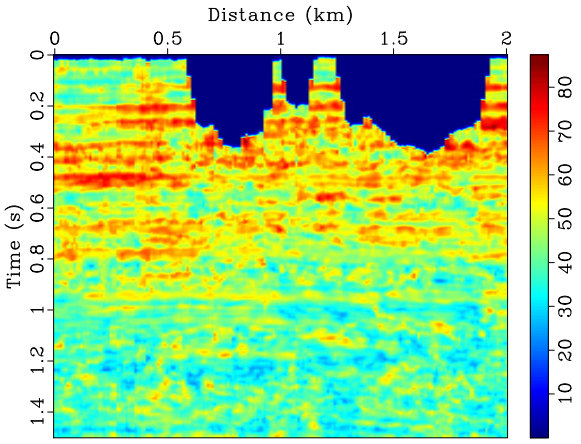

Figure 16: Estimated time-varying average frequency of the field data from time-frequency map.

SHAPING REGULARIZATION FOR INVERSE PROBLEMS

In this appendix, we review the theory of shaping regularization in inversion problems. Fomel (2007b) introduces shaping regularization, a general method of imposing regularization constraints. A shaping operator provides an explicit mapping of the model to the space of acceptable models.

Consider a system of linear equation given as $\mathbf{Ax} = \mathbf{b}$, where $\mathbf{A}$ is a forward-modeling operator, $\mathbf{x}$ is the model, and $\mathbf{b}$ is the data. By equation 8, we can find that the proposed time-frequency decomposition can be written as the form $\mathbf{Ax} = \mathbf{b}$. The standard regularized least-squares approach to solving this equation seeks to minimize $||\mathbf{Ax} = \mathbf{b}||_2^2 + \varepsilon^2 ||\mathbf{Dx}||_2^2$, where $\mathbf{D}$ is the Tikhonov regularization operator (Tikhonov, 1963) and ε is scaling.

The formal solution, denoted by $\hat{\mathbf{x}}$, is given by

$$\hat{x} = \left(\mathbf{A}^T\mathbf{A} + \varepsilon^2\mathbf{D}^T\mathbf{D}\right)^{-1}\mathbf{A}^T\mathbf{b}, \tag{A-1}$$

where $\mathbf{A}^T$ denotes the adjoint operator. Fomel (2007b) defined a relation between a shaping operator S and a regularization operator $\mathbf{D}$ as

$$\mathbf{S} = \left(\mathbf{I} + \varepsilon^2\mathbf{D}^T\mathbf{D}\right)^{-1}. \tag{A-2}$$

Substituting equation A-2 into equation A-1 yields a formal solution of the estimation problem regularization by shaping

$$\hat{\mathbf{x}} = \left(\mathbf{A}^T\mathbf{A} + \mathbf{S}^{-1} - \mathbf{I}\right)^{-1}\mathbf{A}^T\mathbf{b} = \left[\mathbf{I} + \mathbf{S}\left(\mathbf{A}^T\mathbf{A} - \mathbf{I}\right)\right]^{-1}\mathbf{S}\mathbf{A}^T\mathbf{b}. \tag{A-3}$$

Introducing scaling of $\mathbf{A}$ by 1 in equation A-3 , we obtain

$$\hat{\mathbf{x}} = \left[\lambda^2\mathbf{I} + \mathbf{S}\left(\mathbf{A}^T\mathbf{A} - \lambda^2\mathbf{I}\right)\right]^{-1}\mathbf{S}\mathbf{A}^T\mathbf{b}. \tag{A-4}$$

The conjugate-gradient method can be used to compute the inversion in equation A-4 iteratively. As shown by Fomel (2009), the iterative convergence for inversion in equation A-4 can be dramatically faster that the one in equation A-1.

The main advantage of shaping regularization is the relative ease of controlling the selection of λ and $S\mathbf{S}$ in comparison with ε and $\mathbf{D}$ cite[]Fomel2009. In this paper, we choose λ to be the median value of $\mathbf{\Psi_k(t)}$ and the shaping operator to be a Gaussian smoothing operator. The Gaussian smoothing operator is a convolution operator with the Gaussian function that is used to smooth images and remove detail and noise. In this sense it is similar to the mean filter, but it uses a different kernel to represent the shape of a Gaussian (bell-shaped) hump. The Gaussian function in 1D has the form,

$$G(x) = \frac{1}{\sqrt{2\pi\sigma}} \exp\left(-\frac{x^2}{2\sigma^2}\right). \tag{A-5}$$

One can implement Gaussian smoothing by Gaussian filtering in either the frequency domain or time domain. Fomel (2007b) shows that repeated application of triangle smoothing can also be used to implement Gaussian smoothing efficiently, in which case the only additional parameter is the radius of the triangle smoothing operator. In this paper, we use the repeated triangle smoothing operator to implement the Gaussian smoothing operator.

The computational cost of generating a time-frequency representation with our method is $O\left(N_t N_f N_{iter}/N_p\right)$, where N_t is the number of time samples, N_f is the number of frequencies, N_{iter} is the number of conjugate-gradient iterations, N_p is the number of processors used to process different frequencies in parallel, and N_{iter} decreases with the increase of smoothing and is typically around 10.

REFERENCES

Allen, J. G., 1977, Short term spectral analysis, synthetic and modification by discrete Fourier transform: IEEE Transactions on Signal Processing, 135–238.

Brian, C., R. C. Williamson, and B. Boashash, 1993, The relationship between instantaneous frequency and time-frequency representations: IEEE Transactions on Acoustics, Speech, and Signal Processing, **41**, 1458–1461.

Castagna, J., S. Sun, and R. W. Siegfried, 2003, Instantaneous spectral analysis: Detection of low-frequency shadows associated with hydrocarbons: The Leading Edge, **22**, 120–127.

Chakraborty, A., and D. Okaya, 1995, Frequency-time decomposition of seismic data using wavelet-based methods: Geophysics, **60**, 1906–1916.

Claasen, T., and W. Mecklenbruker, 1980, The Wigner distribution – A tool for time-frequency signal analysis, 3 parts: Philips Journal of Research.

Cohen, L., 1989, Time-frequency distributions – A review: Proceedings of the IEEE, **77**, 941–981.

———, 1995, Time-frequency analysis: Prentice Hall, Inc.

Ebrom, D., 2004, The low frequency gas shadows in seismic sections: The Leading Edge, **23**, 772.

Fomel, S., 2007a, Local seismic attributes: Geophysics, **72**, A29–A33.

———, 2007b, Shaping regularization in geophysical-estimation problems: Geophysics, **72**, R29–R36.

———, 2009, Adaptive multiple subtraction using regularized nonstationary regression: Geophysics, **74**, V25–V33.

———, 2010, Predictive painting of 3D seismic volumes: Geophysics, **75**, A25–A30.

Fomel, S., and L. Jin, 2009, Time-lapse image registration using the local similarity attribute: Geophysics, **74**, A7–A11.

Fomel, S., and van der Baan, 2009, Local similarity with the envelope as a seismic phase detector: 80th Annual International Meeting, Soc. of Expl. Geophys., 1555–2559.

Hlawatsch, F., and G. Boudreaux-Bartels, 1992, Linear and quadratic timefrequency signal representations: IEEE Signal Processing Magazine, **9**, 21–67.

Kazemeini, S. H., C. Juhlin, K. Z. Jorgensen, and B. Norden, 2009, Application of the continuous wavelet transform on seismic data for mapping of channel deposits and gas detection at the CO2SINK site, Ketzin, Germany: Geophysical Prospecting, **57**, 111–123.

Korneev, V. A., G. M. Goloshubin, T. M. Daley, and B. S. Dmitry, 2004, Seismic low-frequency effects in monitoring fluid-saturated reservoirs: Geophysics, **69**, 522–532.

Li, Y., and X. Zheng, 2008, Spectral decomposition using Wigner-Ville distribution with applications to carbonate reservoir characterization: The Leading Edge, **27**, 1050–1057.

Liu, G., X. Chen, J. Li, J. Du, and J. Song, 2011a, Seismic noise attenuation using nonstationary polynomial fitting: Applied Geophysics, **8**, 18–26.

Liu, G., S. Fomel, and X. Chen, 2011b, Stacking angle-domain common-image gathers for normalization of illumination: Geophysical Prospecting, **59**, 244–255.

Liu, G., S. Fomel, L. Jin, and X. Chen, 2009, Seismic data stacking using local correction: Geophysics, **74**, V43–V48.

Liu, J., and K. J. Marfurt, 2005, Matching pursuit decomposition using Morlet wavelet: 75th Annual International Meeting, Soc. of Expl. Geophys., 786–789.

Liu, J., Y. Wu, D. Han, and X. Li, 2004, Time-frequency decomposition based on Ricker wavelet: 74th Annual International Meeting, Soc. of Expl. Geophys., 1937–1940.

Liu, Y., and S. Fomel, 2010, Seismic data analysis using local time-frequency transform: 80th Annual International Meeting, Soc. of Expl. Geophys., 3711–3716.

Lomask, J., A. Guitton, S. Fomel, J. Claerbout, and A. Valenciano, 2006, Flattening without picking: Geophysics, **71**, 13–20.

Mallat, S., and Z. Zhang, 1993, Matching pursuit with time-frequency dictionaries: IEEE Transactions on Signal Processing, **41**, 3397–3415.

Margrave, G., 1998, Theory of nonstationary linear filtering in the Fourier domain with application to time-variant filtering: Geophysics, **63**, 244–259.

Partyka, G. A., J. M. Gridley, and J. Lopez, 1998, Interpretational applications of spectral decomposition in reservoir characterization: The Leading Edge, **18**, 353–

360.

Pinnegar, C., and L. Mansinha, 2003, The S-transform with windows of arbitrary and varying shape: Geophysics, **68**, 381–385.

Reine, C., M. van der Baan, and R. Clark, 2009, The robustness of seismic attenuation measurements using fixed- and variable-window time-frequency transforms: Geophysics, **74**, 123–135.

Rioul, O., and M. Vetterli, 1991, Wavelets and signal processing: IEEE Signal Processing Magazine, **8**, 14–38.

Saha, J., 1987, Relationship between Fourier and instantaneous frequency: 57th Annual International Meeting, Soc. of Expl. Geophys., 591.

Sinha, S., P. Routh, and P. Anno, 2009, Instantaneous spectral attributes using scales in continuous-wavelet transform: Geophysics, **74**, WA137–WA142.

Sinha, S., P. S. Routh, P. D. Anno, and J. P. Castagna, 2005, Spectral decomposition of seismic data with continuous-wavelet transform: Geophysics, **70**, P19–P25.

Steeghs, P., and G. Drijkoningen, 2001, Seismic sequence analysis and attribute extraction using quadratic time-frequency representations: Geophysics, **66**, 1947–1959.

Stockwell, R. G., L. Mansinha, and R. P. Lowe, 1996, Localization of the complex spectrum: IEEE Transactions on Signal Processing, **44**, 998–1001.

Tikhonov, A. N., 1963, Solution of incorrectly formulated problems and the regularization method: IEEE Transactions on Signal Processing.

van der Baan, M., and S. Fomel, 2009, Nonstationary phase estimation using regularized local kurtosis maximization: Geophysics, **74**, A75–A80.

Wang, Y., 2007, Seismic time-frequency spectral decomposition by matching pursuit: Geophysics, **72**, V13–V20.

Wigner, E., 1932, On the quantum correction for thermodynamic equilibrium: Physical Review, **40**, 749–759.

Wu, X., and T. Liu, 2009, Spectral decomposition of seismic data with reassigned smoothed pseudo Wigner-Ville distribution: Journal of Applied Geophysics, **68**, 386–393.

Youn, D. H., and J. G. Kim, 1985, Short-time Fourier transform using a bank of low-pass filters: IEEE Transactions on Acoustics, Speech, and Signal Processing, **33**, 182–185.

Zeng, H., M. M. Backus, K. T. Barrow, and N. Tyler, 1998, Stratal slicing, Part I: Realistic 3D seismic model: Geophysics, **63**, 502–513.

Zhenhua, H., X. Xiaojun, and B. Lien, 2008, Numerical simulation of seismic low-frequency shadows and its application: Applied Geophysics, **5**, 301–306.